GPS AUTONOMOUS INTEGRITY MONITORING IN STRAPDOWN-INS/GPS

REN DA AND CHING-FANG LIN
American GNC Corporation, Chatsworth, CA.

Abstract

In this paper, a new failure detection approach is applied for GPS integrity monitoring in an integrated SDINS(strapdown inertial navigation system)/GPS navigation system. In the approach, a bank of auxiliary integrated SDINS/GPS Kalman filters, each of them processing only subsets of the GPS measurements, are applied to provide high accuracy detection references. The failure detection is then undertaken by checking the consistency between the state estimate of the main integrated SDINS/GPS Kalman filter and the auxiliaries. It is shown that the approach is capable of not only detecting the presence of a malfunctioning satellite that results in a large range error, but also identifying which satellite (or satellites) is mulfunctioning.

I. Introduction

Recently, there has been considerable interest in the problem of GPS (Global Positioning System) integrity monitoring [1, 2, 3, 4, 5]. The main concern is over the safety in navigation with GPS and the possibility that a GPS satellite transmits an erroneous navigation signal to the user. Here integrity means the system's ability to provide timely warnings to users as to when it should not be used. It is necessary to apply in advance timely and effective integrity monitoring techniques for occasional large satellite pseudorange errors, because the response time of the GPS Control Segment[4] is typically more than 15 min.

It would be highly desirable for effective Receiver Autonomous Integrity Monitoring (RAIM) to be realized in full within a GPS receiver, taking advantage of satellite redundancy to determine whether the navigation solution is accurate, but experience to date indicates that even a 21-satellite constellation with 3 active spares is unlikely to support receiver autonomous integrity monitoring a large enough fraction of the time for precision approach applications [4].

A new approach suitable for detecting soft failures affecting only subsets of the measurements, such as an erroneous navigation signal from a GPS satellite, was proposed in [6]. In the approach, a bank of auxiliary Kalman filters, each of them processing only subsets of system measurements, are applied to provide high accuracy detection references. The failure detection is then undertaken by checking the consistency between the state estimate of the main Kalman filter and those of the auxiliaries. As an application of this method, the problem of GPS integrity monitoring in a GPS/SDINS(Strapdown Inertial Navigation System) integrated navigation system is investigated in this paper.

The paper is organized as follows: the integrated GPS/SDINS system state and measurement equations are described in Section 2; the general scheme for the GPS automonous integrity monitoring structure in GPS/SDINS systems is presented Section 3; the numerical simulation examples are shown in Section 4; and a brief overall summary is given in Section 5.

II. GPS/SDINS Structure

State Equation

The error states of a GPS/SDINS system are usually of three kinds: 1) those describing the navigation parameter errors; 2) those describing the SDINS error sources, such as the gyro drift and acceleration errors; 3) those describing the GPS error sources, such as the GPS receiver clock offset and clock drift. A complete picture of these errors would involve a large number of states. Due to the restriction of the on-board computation resource, reduced order models have to be applied in practical designs. For the purpose of this analysis, a seventeen-state system is formulated with the error state vector being:

$$\begin{aligned}\mathbf{x}(t) &= [\delta r_N, \delta r_E, \delta r_D, \delta v_N, \delta v_E, \delta v_D, \phi_N, \phi_E, \phi_D, \\ &\quad \Delta_x, \Delta_y, \Delta_z, \varepsilon_x, \varepsilon_y, \varepsilon_z, \delta b, \delta n]^T \end{aligned} \quad (1)$$

where the subscripts "N, E, D" stand for the North-East-Down local level reference frame, and "x, y, z" for the aircraft body reference frame. δr_N, δr_E, δr_D denote the SDINS position errors; δv_N, δv_E, δv_D the SDINS velocity errors; ϕ_N, ϕ_E, ϕ_D the SDINS attitude errors

and azimuth error; Δ_x, Δ_y, Δ_z the accelerometer errors; and ε_x, ε_y, ε_z the gyro errors. δb and δn are the GPS clock offset and clock drift. The SDINS navigation error model is described by the following differential equations [7]

$$\begin{aligned}
\delta\dot{r}_N &= -\dot{\lambda} sinL\, \delta r_E + \dot{L}\, \delta r_D + \delta v_N \\
\delta\dot{r}_E &= \dot{\lambda} sinL\, \delta r_N + \dot{\lambda} cosL\, \delta r_D + \delta v_E \\
\delta\dot{r}_D &= -\dot{L}\, \delta r_N - \dot{\lambda} cosL\, \delta r_E - c_1\, \delta r_D + \delta v_D \\
\delta\dot{v}_N &= -\frac{f_D + g}{R}\delta r_N + \frac{f_E tanL}{R}\delta r_E - (2\Omega + \dot{\lambda}) \\
&\quad \times sinL\delta v_E + \dot{L}\delta v_D - f_D\phi_E + f_E\phi_D + \Delta_N \\
\delta\dot{v}_E &= -\frac{f_D + g + f_N tanL}{R}\delta r_E + (2\Omega + \dot{\lambda}) sinL\delta v_N \\
&\quad + (2\Omega + \dot{\lambda}) cosL\delta v_D + f_D\phi_N - f_N\phi_D + \Delta_E \\
\delta\dot{v}_D &= \frac{f_N}{R}\delta r_N + \frac{f_E}{R}\delta r_E + (\frac{2g}{R} - c_2)\delta r_D - \dot{L}\delta v_N \\
&\quad - (2\Omega + \dot{\lambda}) cosL\delta v_E - f_E\phi_N + f_N\phi_E + \Delta_D \\
\dot{\phi}_N &= -\frac{\Omega sinL}{R}\delta r_N + (\frac{v_D}{R^2} + \frac{\dot{L} tanL}{R})\delta r_E \\
&\quad + \frac{\dot{\lambda} cosL}{R}\delta r_D + \frac{1}{R}\delta v_E - (\Omega + \dot{\lambda}) sinL\phi_E \\
&\quad + \dot{L}\phi_D + \varepsilon_N \qquad (2) \\
\dot{\phi}_E &= -\frac{v_D}{R^2}\delta r_N + \frac{\dot{\lambda} sinL}{R}\delta r_E - \frac{\dot{L}}{R}\delta r_D - \frac{1}{R}\delta v_N \\
&\quad + (\Omega + \dot{\lambda}) sinL\phi_N + (\Omega + \dot{\lambda}) cosL\phi_D + \varepsilon_E \\
\dot{\phi}_D &= -(\frac{\Omega cosL}{R} + \frac{\dot{\lambda}}{RcosL})\delta r_N - \frac{tanL}{R}(\dot{L} tanL \\
&\quad + \frac{v_D}{R})\delta r_E - \frac{\dot{\lambda} sinL}{R}\delta r_D - \frac{tanL}{R}\delta v_E \\
&\quad - \dot{L}\phi_N - (\Omega + \dot{\lambda}) cosL\phi_E + \varepsilon_D
\end{aligned}$$

where λ and L are the longitude and latitude angles; R the radius of the Earth, and Ω its angular rate; f the specific force measured by the accelerometers; and c_1 and c_2 are the damping gains introduced by the altimeter damping loop of the vertical channel. The input axes of the strapped-down gyros and accelerometers are assumed to be aligned with the principal axes of the aircraft. Δ_N, Δ_E, Δ_D, and ε_N, ε_E, ε_D are, respectively, the errors of the accelerometers and gyros mapped from the aircraft body frame into the navigation frame, using appropriate elements of the direction cosine matrix. The accelerometer and gyro errors in the aircraft body frame are modeled as the combination of a random bias, a white random process and a random walk process. Therefore we have

$$\begin{aligned}
\dot{\Delta}_i &= w_{\Delta i} \qquad (i = x, y, z) \\
\dot{\varepsilon}_i &= w_{\varepsilon i} \qquad (i = x, y, z) \qquad (3)
\end{aligned}$$

where w_Δ and w_ε are white input noise processes. The GPS clock offset and drift are modeled by the following equations:

$$\begin{aligned}
\delta\dot{b} &= -\tau_b\delta b + \delta n + w_b \\
\delta\dot{n} &= -\tau_n\delta n + w_n \qquad (4)
\end{aligned}$$

where τ_b and τ_n are time-constants, w_b and w_n white input noises.

Measurement Equation

Based on the position data indicated by the SDINS and the ephemeris data from the GPS receiver, the ranges from the aircraft to the four satellites being tracked can be calculated. The Kalman filter measurements y_i, $(i = 1, 2, 3, 4)$ are formed by the differences between the pseudoranges provided by the GPS receiver and the calculated ranges. Therefore, we have the following measurement equations:

$$\begin{aligned}
y_i &= cos\alpha_i\delta r_N + cos\beta_i\delta r_E + cos\gamma_i\delta r_D + \delta b + d_i + v_i \\
&\qquad (i = 1, 2, 3, 4) \qquad (5)
\end{aligned}$$

where $(cos\alpha_i, cos\beta_i, cos\gamma_i)$ are the direction cosines between the line-of-sight from the ith satellite to the aircraft and the navigation frame, d_i the pseudorange error resulting from the satellite failure, and v_i the pseudorange measurement white noise.

III. GPS Integrity Monitoring Structure

A GPS integrity monitoring system based on the previously discussed failure detection approach is illustrated in Figure 1, where the main Kalman filter $\mathcal{A}$ processes all the four measurements to generate the best state estimate $\hat{\mathbf{x}}^{\mathcal{A}}$ and its covariance $P^{\mathcal{A}}$; each of the auxiliary Kalman filters processes three out of the four measurements to provide the state estimates $\hat{\mathbf{x}}^j$ (the superscript $j = \mathcal{B}, \mathcal{C}, \mathcal{D}, \mathcal{E}$) and their covariances P^j for consistency checking. The measurement vectors for the Kalman filters are as follows:

$$\mathbf{y}^{\mathcal{A}}(k) = \begin{pmatrix} y_1 \\ y_2 \\ y_3 \\ y_4 \end{pmatrix} \quad \mathbf{y}^{\mathcal{B}}(k) = \begin{pmatrix} y_1 \\ y_2 \\ y_3 \end{pmatrix} \quad \mathbf{y}^{\mathcal{C}}(k) = \begin{pmatrix} y_1 \\ y_2 \\ y_4 \end{pmatrix}$$

$$\mathbf{y}^{\mathcal{D}}(k) = \begin{pmatrix} y_1 \\ y_3 \\ y_4 \end{pmatrix} \quad \mathbf{y}^{\mathcal{E}}(k) = \begin{pmatrix} y_2 \\ y_3 \\ y_4 \end{pmatrix} \qquad (6)$$

It is proven in [6] that the estimation differences between the Kalman filter $\mathcal{A}$ and the others:

$$\mathbf{b}^j(k) = \hat{\mathbf{x}}^j(k|k) - \hat{\mathbf{x}}^{\mathcal{A}}(k|k) \qquad (7)$$

are zero mean Gaussian vectors with covariances

$$B^j(k) = E\{\mathbf{b}^j(k)[\mathbf{b}^j(k)]^T\} = P^j(k|k) - P^{\mathcal{A}}(k|k) \quad (8)$$

when there is no failure. Then the GPS integrity can be monitored based on the hypotheses $H_0 : \mathbf{b}^j(k) \sim N[0, B^j(k)]$ subject to the false alarm probability γ.

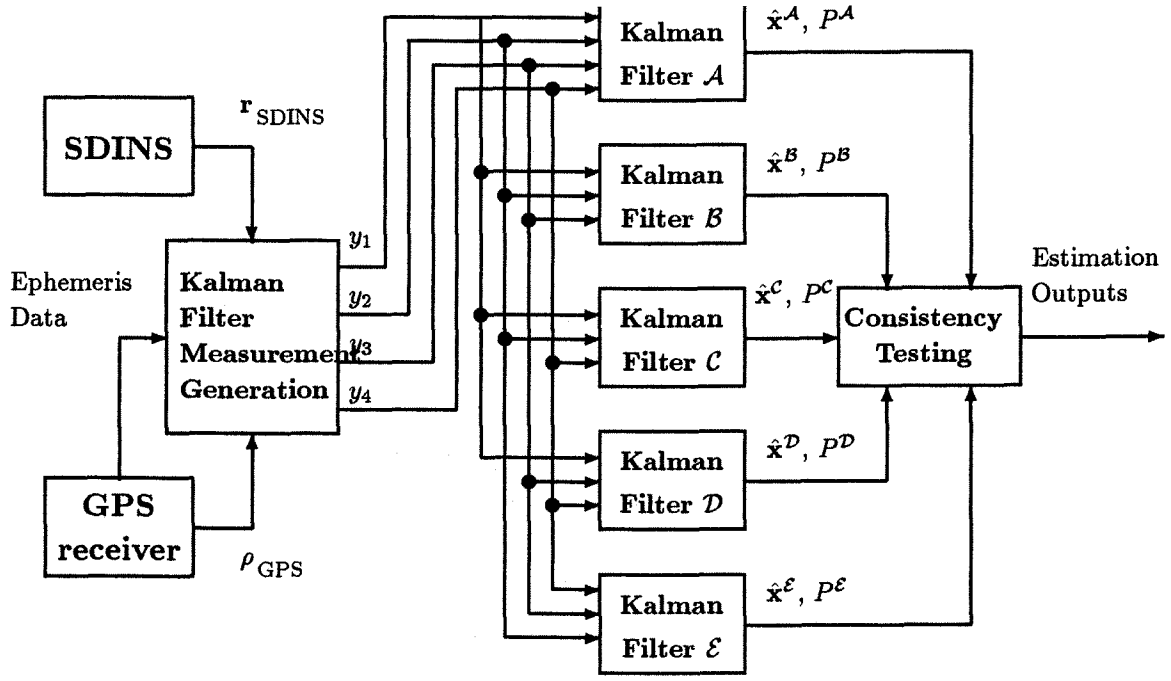

Figure 1: A GPS Integrity Monitoring System Structure

If a satellite being tracked fails, one of the auxiliary Kalman filters remains uncontaminated and so at least one of the consistency tests is expected to signal an alarm.

Statistical Hypothesis Test

Based on the above discussion, we have $\mathbf{b}^j \sim N[0, B^j(k)]$ when there is no failure. A failure will cause the expectation of $\mathbf{b}^j$ to become non-zero and/or its covariance larger than $B^j(k)$. Therefore, failure detection can be performed by standard statistical testing techniques between the hypotheses:

$$\begin{aligned} H_0: &\quad \mathbf{b}^j(k) \sim N[0, B^j(k)] \\ H_1: &\quad H_0 \text{ not true} \end{aligned} \tag{9}$$

subject to the false alarm probability

$$Pr[\text{ accept } H_1 \mid H_0 \text{ true }] = \gamma \tag{10}$$

A simple and effective testing approach for our case is the chi-square test. From the fact that the normalized sequence

$$\lambda^j(k) \triangleq [\mathbf{b}^j(k)]^T [B^j(k)]^{-1} \mathbf{b}^j(k) \sim \chi^2(n) \tag{11}$$

is chi-square distributed with n degrees of freedom [8] (where n is the dimension of $\mathbf{b}^j$), we have the following detection rule:

$$\zeta^j \triangleq \frac{\lambda^j}{\epsilon^j} \begin{cases} \geq 1 & \text{means failure} \\ < 1 & \text{means no failure} \end{cases} \tag{12}$$

where ζ^j is the scaled test statistic and ϵ^j the threshold obtained from the chi-square distribution table with the chosen false alarm probability γ.

Equation (11) considers the whole vector $\mathbf{b}^j(k)$ as the testing object, with the advantage of including the cross correlation among the components of $\mathbf{b}^j(k)$. But for high dimensional systems, the method may suffer two drawbacks: (1) the difficulty associated with the matrix inversion calculation; (2) the low detection sensitivity to failures affecting only one or few components of $\mathbf{b}^j(k)$ (note that the threshold ϵ^j increases with n). These drawbacks can be avoided by testing the components of $\mathbf{b}^j$ individually as

$$\lambda_l^j(k) \triangleq \frac{[b_l^j(k)]^2}{B_{ll}^j(k)} \sim \chi^2(1) \tag{13}$$

where $b_l^j(k)$ and $B_{ll}^j(k)$ are, respectively, the i th component of $\mathbf{b}^j(k)$ and the diagonal component of $B^j(k)$. The corresponding detection rule is:

$$\zeta_l^j \triangleq \frac{\lambda_l^j}{\epsilon_l^j} \begin{cases} \geq 1 & \text{means failure} \\ < 1 & \text{means no failure} \end{cases} \tag{14}$$

with the threshold ϵ_l^j again obtained from the chi-square distribution table with the chosen false alarm probability. With this detection rule, we can expect that the test statistic of $\zeta_l^j(k)$, which is most seriously affected by the failures, flags the failures first.

Sometimes, testing two or more closely related components of $\mathbf{b}^j(k)$ together may yield higher failure detection sensitivity than testing them individually, if they are seriously affected by the same failure at the same time. In these cases, we can use the elements of the covariance matrix $B^j(k)$, which are related to the components to be tested, to form suitable test statistics.

For example, b_1^j and b_2^j are readily tested together since

$$\lambda_{12}^j = (b_1^j \quad \beta_2^j) \begin{pmatrix} B_{1,1} & B_{1,2} \\ B_{2,1} & B_{2,2} \end{pmatrix}^{-1} \begin{pmatrix} b_1^j \\ b_2^j \end{pmatrix} \sim \chi^2(2) \tag{15}$$

IX. Simulation Results

In simulation, the components of $\mathbf{b}^j$ were tested separately and the scaled test statistics were used. All the thresholds were chosen as $\epsilon = 7.87944$, corresponding to a false alarm probability of 0.005. Table 1 lists the initial variances and parameters of the error states to be used in the simulation analysis. The mission scenario was 2000 seconds of flight towards west at a constant flight speed of 300 m/s.

Simulation Results without SA

The effectiveness of the GPS integrity monitoring system was first investigated without considering the Selective Availability (SA). It was assumed that the failures in satellite 1 resulted in the following two kinds of ramp-type pseudorange errors:

- *Case 1*:

$$d_1 = \begin{cases} 0\ m & 0\ s \le t < 1000\ s \\ 3(t-1000)\ m & 1000\ s \le t < 1010\ s \\ 30\ m & 1010\ s \le t \le 2000\ s \end{cases} \tag{16}$$

- *Case 2*:

$$d_1 = \begin{cases} 0\ m & 0\ s \le t < 1000\ s \\ 0.3(t-1000)\ m & 1000\ s \le t < 1100\ s \\ 30\ m & 1100\ s \le t \le 2000\ s \end{cases} \tag{17}$$

Our discussion will concentrate on the consistency testing results associated with the main Kalman filter $\mathcal{A}$ and the auxiliary filter $\mathcal{E}$ which is the only one uncontaminated when the satellite 1 fails, and on the results related to the position errors which are not only the most important parameters for practical navigation systems, but also those most seriously affected by the GPS pseudorange failures. The results related to most of the other error states will be omitted for better clarity.

Figure 2 shows the real north-position estimation errors $\tilde{\delta r}_N^{\mathcal{A}}$ in the failure *Case 1* (solid line) and *Case 2* (dashed line), as well as the standard derivation $\sqrt{P_{\delta r_N}^{\mathcal{A}}}$ from the Kalman filter $\mathcal{A}$. Under normal working status ($t \le 1000\ s$), the $\tilde{\delta r}_N^{\mathcal{A}}$ is mainly limited within the scope $\pm\sqrt{P_{\delta r_N}^{\mathcal{A}}}$. Once the failures happen at $t = 1000$ s, the $\tilde{\delta r}_N^{\mathcal{A}}$ increases rapidly and soon exceeds that scope for both *Case 1* and *Case 2*.

Table 1: The Modeling Parameter List

Error Source	Value ($1\ \sigma$)	Units
Initial position errors		
$\delta r_N, \delta r_W, \delta r_Z$	100.0	m
Initial velocity errors		
$\delta v_N, \delta v_W, \delta v_Z$	1.0	m/s
Initial attitude errors		
ϕ_N, ϕ_W	300.0	$arc\ sec$
Initial azimuth error ϕ_Z	900.0	$arc\ sec$
Acc. errors $\Delta_x, \Delta_y, \Delta_z$	500.0	μg
Acc. white noise	5.0	$\mu g * s^{1/2}$
Gyro errors $\varepsilon_x, \varepsilon_y, \varepsilon_z$	0.1	deg/h
Gyro white noise	0.001	$deg/h^{1/2}$
GPS clock offset bias	30	m
GPS clock offset noise w_b	0.1	$m * s^{1/2}$
GPS clock drift δn	0.03	m/s
GPS pseudorange noise	10	m

The real state estimation errors are not known in the practical Kalman filter systems because the real system states are not known. Hence, some kind of reference systems are always needed in order to monitor the real estimation errors indirectly. Figure 3 indicates that the Kalman filter $\mathcal{E}$, not contaminated by the failed measurement y_1, provides an excellent reference system. Using three out of the four pseudorange measurements, the accuracy of the Kalman filter $\mathcal{E}$ is fairly high. The difference between the covariance $P_{\delta r_N}^{\mathcal{E}}$ and $P_{\delta r_N}^{\mathcal{A}}$, for example, is less than (5 m)^2 after a short filtering time (t > 300 s). Therefore the plots of $b_{\delta r_N}^{\mathcal{E}}$

$$b_{\delta r_N}^{\mathcal{E}} = \hat{\delta r}_N^{\mathcal{E}} - \hat{\delta r}_N^{\mathcal{A}} = \tilde{\delta r}_N^{\mathcal{A}} - \tilde{\delta r}_N^{\mathcal{E}} \tag{18}$$

behave like $\tilde{\delta r}_N^{\mathcal{A}}$, because

$$\tilde{\delta r}_N^{\mathcal{A}} >> \tilde{\delta r}_N^{\mathcal{E}} \quad \text{and} \quad b_{\delta r_N}^{\mathcal{E}} \approx \tilde{\delta r}_N^{\mathcal{A}} \tag{19}$$

after the failures happen.

In the practical applications, it is often desirable to know approximately the scopes of the real state estimation errors, in order to decide the seriousness of the failures detected. This can be done on the basis of the information provided by the Kalman filters. For example, the scope of the real north-position estimation error can be estimated by the following inequality

$$\begin{aligned} |\tilde{\delta r}_N^{\mathcal{A}}| &= |\delta r_N - \hat{\delta r}_N^{\mathcal{A}}| \\ &\le |\delta r_N - \hat{\delta r}_N^{\mathcal{E}}| + |\hat{\delta r}_N^{\mathcal{E}} - \hat{\delta r}_N^{\mathcal{A}}| \\ &< 3\sqrt{P_{\delta r_N}^{\mathcal{E}}} + |\hat{\delta r}_N^{\mathcal{E}} - \hat{\delta r}_N^{\mathcal{A}}| \end{aligned} \tag{20}$$

Thus the maximum $|\tilde{\delta r}_N^{\mathcal{A}}|$ is calculated to be less than 45 m in both failure cases, based on the data of $\hat{\delta r}_N^{\mathcal{A}}$, $P_{\delta r_N}^{\mathcal{E}}$ and $\hat{\delta r}_N^{\mathcal{E}}$ from the filter $\mathcal{A}$ and $\mathcal{E}$.

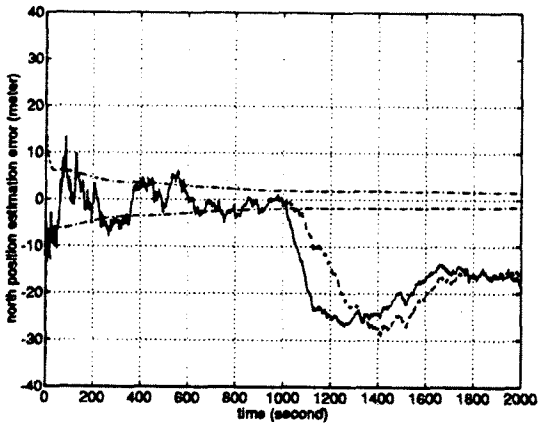

Figure 2: The $\tilde{\delta r}_N^{\mathcal{A}}$ at the failure case 1 (solid line) and case 2 (dash line), as well as $\pm\sqrt{P_{\delta \mathbf{r}_N}^{\mathcal{A}}}$ (dashdot lines).

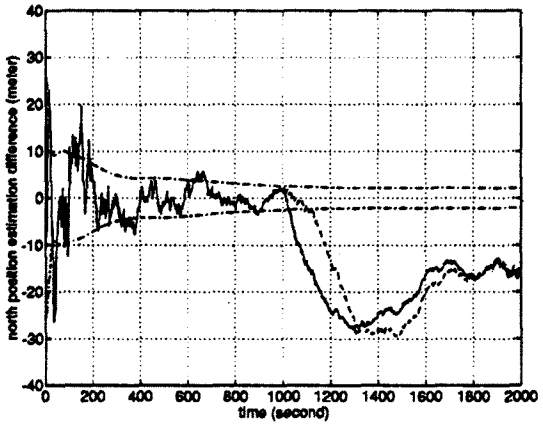

Figure 3: The $\hat{\delta r}_N^{\mathcal{E}} - \hat{\delta r}_N^{\mathcal{A}}$ at the failure *case 1* (solid line) and *case 2* (dash line), as well as the $\pm\sqrt{P_{\delta \mathbf{r}_N}^{\mathcal{E}} - P_{\delta \mathbf{r}_N}^{\mathcal{A}}}$ (dashdot lines).

Figure 4 plots the consistency testing results of the north-position error for both failure cases. As expected, the scaled chi-square test statistics $\zeta_{\delta r_N}^{\mathcal{E}}$

$$\zeta_{\delta r_N}^{\mathcal{E}} = \frac{(\hat{\delta r}_N^{\mathcal{A}} - \hat{\delta r}_N^{\mathcal{E}})^2}{\epsilon(P_{\delta r_N}^{\mathcal{E}} - P_{\delta r_N}^{\mathcal{A}})} \tag{21}$$

increase rapidly with accumulation of the failure effects on the north-position estimation. When the scaled chi-square test statistics $\zeta_{\delta r_N}^{\mathcal{E}}$ are larger than 1, the failures are declared, e.g., the failure alarm signals are given, respectively, at t = 1040 s for the failure *Case 1* and t = 1160 s for the failure *Case 2*. For both failure cases, the real estimation errors $\tilde{\delta r}_N^{\mathcal{A}}$ are less than 10 m, when the failures are declared. Hence the failure detection system is quite sensitive to the GPS pseudorange failures, which are detected well before large position estimation errors result.

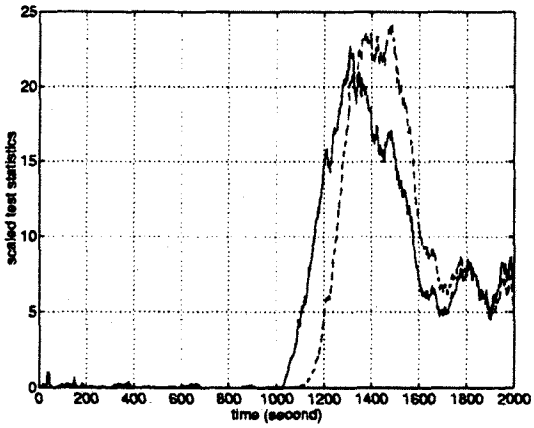

Figure 4: The $\zeta_{\delta \mathbf{r}_N}^{\mathcal{E}}$ at the failure *case 1* (solid line) and *case 2* (dash line). ($\zeta_{\delta \mathbf{r}_N}^{\mathcal{E}} = (\hat{\delta \mathbf{r}}_N^{\mathcal{A}} - \hat{\delta \mathbf{r}}_N^{\mathcal{E}})^2/(P_{\delta \mathbf{r}_N}^{\mathcal{E}} - P_{\delta \mathbf{r}_N}^{\mathcal{A}})$).

Simulation Results with SA

The effectiveness of the GPS integrity monitoring system was also investigated under consideration of the Selective Availability (SA) implemented in the newer Block II GPS satellites. SA controls the accuracy of the Standard Positioning Service (SPS) signals by the combination of dithering the satellite clock and manipulating the ephemeris data. While the former causes a quickly varying satellite pseudorange error with limited amplitude, the latter results in a very large but slowly varying bias.

The effects of SA were considered by modeling the pseudorange errors due to it, for each of the satellites being tracked, as a first order Markov process $\delta \dot{s}_i$:

$$\delta \dot{s}_i = -\tau_s \delta s_i + w_{si} \quad (i = 1, 2, 3, 4) \tag{22}$$

where τ_s is a time constant and w_{si} the white input noise. Then we have the following error state vector:

$$\begin{aligned} \mathbf{x}(t) \;=\; & [\delta r_N, \delta r_E, \delta r_D, \delta v_N, \delta v_E, \delta v_D, \phi_N, \phi_E, \phi_D, \\ & \Delta_x, \Delta_y, \Delta_z, \varepsilon_x, \varepsilon_y, \varepsilon_z, \delta b, \delta n, \delta s_1, \delta s_2, \delta s_3, \delta s_4]^T \end{aligned} \tag{23}$$

The measurement equations of (5) now read:

$$\begin{aligned} y_i \;=\; & cos\alpha_i \delta r_N + cos\beta_i \delta r_E + cos\gamma_i \delta r_D \\ & + \delta b + \delta s_i + c_i + v_i \quad (i = 1, 2, 3, 4) \end{aligned} \tag{24}$$

In the simulation analysis, the associated standard deviations of SA was chosen as 30 m and again two soft ramp-type failure cases were considered:

- *Case 3*:

$$d_1 = \begin{cases} 0\ m & 0\ s \le t < 1000\ s \\ 3(t - 1000)\ m & 1000\ s \le t < 1100\ s \\ 300\ m & 1100\ s \le t \le 2000\ s \end{cases} \tag{25}$$

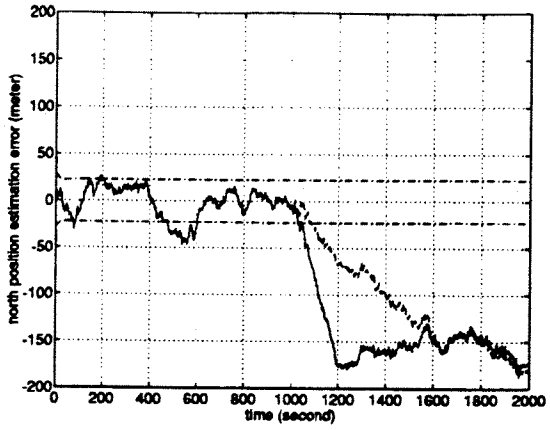

Figure 5: The $\tilde{\delta r}_N^{\mathcal{A}}$ at the failure *case 3* (solid line) and *case 4* (dash line), as well as the $\pm\sqrt{P^{\mathcal{A}}_{\delta \mathbf{r}_N}}$ (dashdot lines), with the SA.

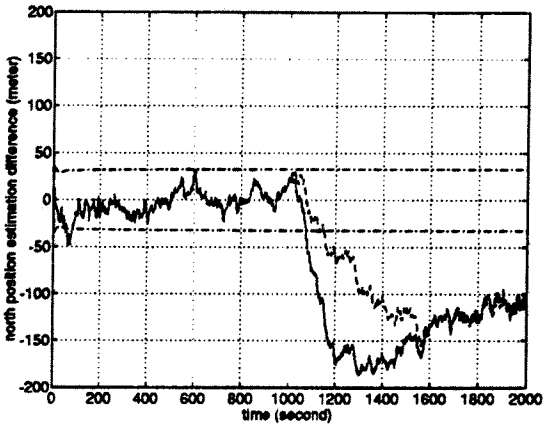

Figure 6: The $\hat{\delta \mathbf{r}}_N^{\mathcal{E}} - \hat{\delta \mathbf{r}}_N^{\mathcal{A}}$ at the failure *case 3* (solid line) and *case 4* (dash line), as well as the $\pm\sqrt{P^{\mathcal{E}}_{\delta \mathbf{r}_N} - P^{\mathcal{A}}_{\delta \mathbf{r}_N}}$ (dashdot lines), with the SA.

- *Case 4*:

$$d_1 = \begin{cases} 0\ m & 0\ s \le t < 1000\ s \\ (t - 1000)\ m & 1000\ s \le t < 1300\ s \\ 300\ m & 1300\ s \le t \le 2000\ s \end{cases} \tag{26}$$

Figure 5 shows that the real north-position estimation errors $\tilde{\delta r}_N^{\mathcal{A}}$ in *Case 3* (solid line) and *Case 4* (dashed line) far exceed the scope defined by $\pm\sqrt{P^{\mathcal{A}}_{\delta r_N^{\mathcal{A}}}}$ after the failures happen. Figure 6 demonstrates the estimation differences between $\hat{\delta r}_N^{\mathcal{E}}$ and $\hat{\delta r}_N^{\mathcal{A}}$ and the scope defined by the $\pm\sqrt{P^{\mathcal{E}}_{\delta r_N} - P^{\mathcal{A}}_{\delta r_N}}$, which is still less than 40 m even under the effects of SA. Therefore, $b^{\mathcal{E}}_{\delta r_N}$ can still fairly accurately approximate the real estimation error $\tilde{\delta r}_N^{\mathcal{A}}$ when the failures result in large estimation errors. Figure 7 plots the scaled chi-square test statistics $\zeta^{\mathcal{E}}_{\delta r_N}$ for the two failure cases. The failure alarm signals are given at t = 1110 *s* for the failure *Case 3* and t = 1280 *s* for the failure *Case 4* respectively. In both cases, when the failures are declared the real estimation errors of $\tilde{\delta r}_N^{\mathcal{A}}$ are less than 80 m. Therefore the system functions pretty well even when SA is considered. The failures can be detected well before large position estimation errors result.

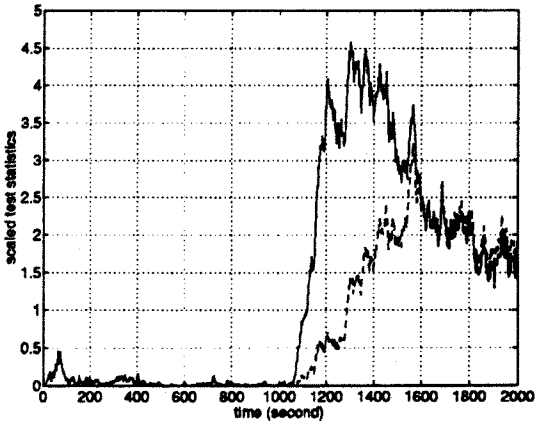

Figure 7: The $\zeta^{\mathcal{E}}_{\delta \mathbf{r}_N}$ at the failure *case 3* (solid line) and *case 4* (dash line), with the SA ($\zeta^{\mathcal{E}}_{\delta \mathbf{r}_N} = (\hat{\delta \mathbf{r}}_N^{\mathcal{A}} - \hat{\delta \mathbf{r}}_N^{\mathcal{E}})^2/(P^{\mathcal{E}}_{\delta \mathbf{r}_N} - P^{\mathcal{A}}_{\delta \mathbf{r}_N})$).

Discussions

It should be pointed out that in addition to the test statistics of position errors, those of certain other error states can also flag satellite failures and perhaps even earlier. As an example, the scaled chi-square test statistic $\zeta^{\mathcal{E}}_{\delta n}$ of the GPS clock drift

$$\zeta^{\mathcal{E}}_{\delta n} = \frac{(\hat{\delta n}^{\mathcal{A}} - \hat{\delta n}^{\mathcal{E}})^2}{\epsilon(P^{\mathcal{E}}_{\delta n} - P^{\mathcal{A}}_{\delta n})} \tag{27}$$

is shown in Figure 8. Physically, it is understood that the estimation error of the clock drift is related to the velocity estimation errors, or the change rates of the position estimation errors. This is also true for the $\zeta^{\mathcal{E}}_{\delta n}$. Figures 5 and 8 show that the magnitude of $\zeta^{\mathcal{E}}_{\delta n}$ is clearly related to the change rate of the north-position error. The larger the rate and the longer the time of the position errors increase, the larger the $\zeta^{\mathcal{E}}_{\delta n}$. The dependence of $\zeta^{\mathcal{E}}_{\delta n}$ on the change rate of the position estimation errors can also be observed when comparing the plots of the $\zeta^{\mathcal{E}}_{\delta n}$ in *Case 3* and *Case 4*, as shown in Figure 8. The maximum response of $\zeta^{\mathcal{E}}_{\delta n}$ in *Case 3* is much larger than in *Case 4*, because the increasing rate of the position estimation in *Case 3* is much larger than that in *case 4*. By contrast, the maximum difference in the $\zeta^{\mathcal{E}}_{\delta r_N}$ for the two cases is less significant (Figure 7) as the maximum difference in the $\tilde{\delta r}_N^{\mathcal{A}}$ is small (Figure 6).

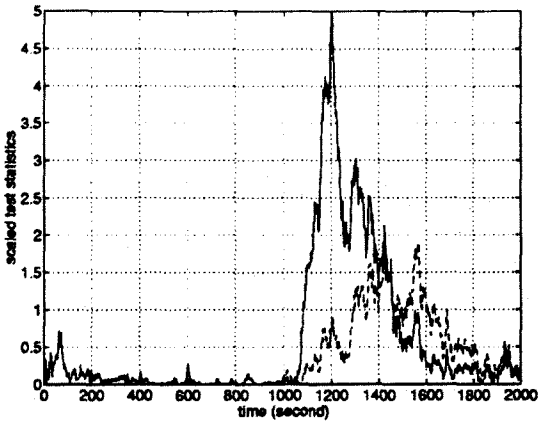

Figure 8: The $\zeta^{\mathcal{E}}_{\delta n}$ at the failure *case 3* (solid line) and *case 4* (dash line), with the SA ($\zeta^{\mathcal{E}}_{\delta n} = (\hat{\delta n}^{\mathcal{A}}_N - \hat{\delta n}^{\mathcal{E}}_N)^2/(P^{\mathcal{E}}_{\delta n_N} - P^{\mathcal{A}}_{\delta n_N})$).

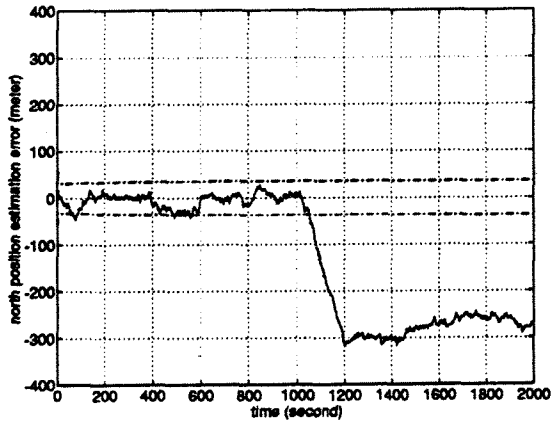

Figure 9: The $\tilde{\delta \mathbf{r}}^{\mathcal{B}}_N$ at the failure *case 3* and the $\pm\sqrt{P^{\mathcal{B}}_{\delta \mathbf{r}_N}}$ (dashdot lines) with the SA.

Since $\zeta^{\mathcal{E}}_{\delta n}$ is sensitive to the increasing rate of the position estimation error rather than to its magnitude, as $\zeta^{\mathcal{E}}_{\delta r_N}$ is, the plots of $\zeta^{\mathcal{E}}_{\delta n}$ look highly noisy. Depending on the seriousness of the failures, $\zeta^{\mathcal{E}}_{\delta n}$ may declare a failure earlier than $\zeta^{\mathcal{E}}_{\delta n}$ does, as shown in Figure 8. It may also miss flagging the failures which only result in slow change of the position estimation errors.

It should be also pointed out that not only the consistency tests between the Kalman filters $\mathcal{A}$ and $\mathcal{E}$, but also those between the Kalman filter $\mathcal{A}$ and others may signal failures. Figure 9, for example, shows that even though the filters $\mathcal{A}$ and $\mathcal{B}$ are affected by the same satellite failure (*Case 3*), the resulting north-position estimation error has a large difference. The maximum value of the $|\tilde{\delta r}^{\mathcal{B}}_N|$ is almost two times that of the $|\tilde{\delta r}^{\mathcal{A}}_N|$ (Figure 5). Therefore, the estimation difference between $\hat{\delta r}^{\mathcal{B}}_N$ and $\hat{\delta r}^{\mathcal{B}}_N$ is large enough to cause the scaled test statistics $\zeta^{\mathcal{B}}_{\delta rN}$ to signal the failure, as shown in Figure 10.

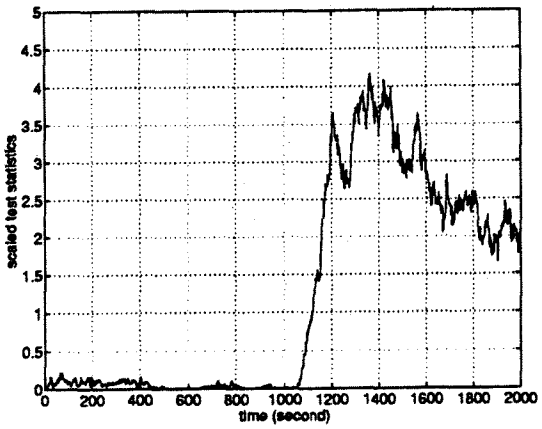

Figure 10: The $\zeta^{\mathcal{B}}_{\delta \mathbf{r}_N}$ at the failure *case 3* with the SA ($\zeta^{\mathcal{B}}_{\delta \mathbf{r}_N} = (\hat{\delta \mathbf{r}}^{\mathcal{A}}_N - \hat{\delta \mathbf{r}}^{\mathcal{B}}_N)^2/(P^{\mathcal{B}}_{\delta \mathbf{r}_N} - P^{\mathcal{A}}_{\delta \mathbf{r}_N})$).

Conclusion

A new approach for detecting system failures which affect only subsets of system measurements was applied for GPS integrity monitoring in an integrated SDINS(strapdown inertial navigation system)/GPS navigation system. It exploits the concepts of using a bank of auxiliary integrated GPS/SDINS Kalman filters, which process subsets of GPS measurements, as highly accurate failure detection references, and detecting GPS failures by checking the consistency between the state estimate of the main integrated GPS/SDINS Kalman filter and those of the auxiliaries. Simulation results demonstrate that even in the presence of the Selective Availability, the soft ramp-type GPS satellite failures are successfully declared. More important, however, is the fact that GPS failures are detected well before large position estimation errors result. Therefore, it is quite plausible for the GPS autonomous monitoring system to meet non-precision landing approach requirements.

Acknowledgments

This paper describes research partly accomplished by the first author at the Technion - Israel Institute of Technology, Israel, where he was supported by a post-doctoral Fellowship from the Israel Council of Higher Education. The authors would like to thank Prof. I. Y. Bar-Itzhack of the Technion for his comments and suggestions.

References

[1] G. Brown and P. C. Hwang, "GPS failure detection by autonomous means within the cockpit,"

Navigation: Journal of the Institute of Navigation, vol. 33, no. 4, pp. 335–353, 1986.

[2] R. Braff and C. Shively, "GPS integrity channel," *Navigation: Journal of the Institute of Navigation*, vol. 32, no. 4, pp. 334–350, 1985.

[3] P. S. Jorgensen, "Achieving GPS integrity and eliminating areas of degraded performance," *Navigation: Journal of the Institute of Navigation*, vol. 34, no. 4, pp. 297–306, 1987.

[4] R. H. Kalafus, "GPS integrity channel RTCA working group recommendations," *Navigation: Journal of Institute of Navigation*, vol. 36, no. 1, pp. 25–44, 1989.

[5] M. A. Sturza, "Navigation system integrity monitoring using redundant measurements," *Navigation: Journal of the Institute of Navigation*, vol. 35, no. 4, pp. 483–501, 1988.

[6] R. Da and C. F. Lin, "A New Failure Detection Approach and its Application to GPS Autonomous Integrity Monitoring," *Submitted to IEEE Transactions on Aerospace System and Electronic Systems*, 1994.

[7] I. Y. Bar-Itzhack, "Minimal order time sharing filters for INS in-flight alignment," *Journal of Guidance and Control*, vol. 5, no. 4, pp. 396–402, 1982.

[8] W. Mendenhall and T. Sincich, *Statistics for Engineering and the Science*. San Francisco: Dellen, 5 ed., 1992.

[9] C. F. Lin, *Modern Navigation, Guidance, and Control Processing*. Englewood Cliffs, New Jersey: Prentice-Hall Series in Advanced Navigation, Guidance, and Control, and their Applications, Prentice-Hall, 1991.

[10] C. F. Lin (*ed*), *Advanced Control System Design*. Englewood Cliffs, New Jersey: Prentice-Hall Series in Advanced Navigation, Guidance, and Control, and their Applications, Prentice-Hall, 1994.

[11] R. Da, "Failure Detection of Dynamical Systems with State Chi-Square Test," *AIAA Journal of Guidance, Control, and Dynamics*, vol. 17, no. 2, pp. 271–277, 1994.

[12] A. S. Willsky, "A survey of design methods for failure detection in dynamic systems," *Automatica*, vol. 12, pp. 601–611, 1976.

[13] R. Isermann, "Process fault detection based on modeling and estimation methods–a survey," *Automatica*, vol. 20, no. 4, pp. 387–404, 1984.

[14] T. H. Kerr, "Decentralized Kalman filtering and redundancy management for multisensor navigation," *IEEE Transactions on Aerospace and Electronic Systems*, vol. 23, no. 1, pp. 83–119, 1987.

[15] P. M. Frank, "Fault diagnosis in dynamic system using analytical and knowledge-based redundancy - a survey and some new results," *Automatica*, vol. 26, no. 1, pp. 459–474, 1990.

[16] P. S. Maybeck, *Stochastic models, estimation, and control*. Vol. 1, New York: Academic Press, 1979.

[17] R. K. Mehra and J. Peschon, "An innovations approach to fault detection and diagnosis in dynamic systems," *Automatica*, vol. 7, pp. 637–640, 1971.

[18] T. H. Kerr, "Real-time failure detection: a static nonlinear optimization problem that yields a two ellipsoid overlap test," *Journal of Optimization Theory and Application*, vol. 20, no. 4, pp. 509–536, 1977.

[19] T. H. Kerr, "Statistical analysis of a two-ellipsoid overlap test for real-time failure detection," *IEEE Transactions on Automatic Control*, vol. 25, no. 4, pp. 762–772, 1980.

[20] B. D. Brumback and M. D. Srinath, "Fault-tolerant multisensor navigation system design," *IEEE Transactions on Aerospace and Electronic Systems*, vol. 23, no. 6, pp. 738–755, 1987.